

## Coordinated Followup Could Have Enabled the Discovery of the GW190425 Kilonova

IDO KEINAN<sup>1</sup> AND IAIR ARCAVI<sup>1</sup>

<sup>1</sup>*The School of Physics and Astronomy, Tel Aviv University, Tel Aviv 69978, Israel*

### ABSTRACT

The discovery of a kilonova associated with the GW170817 binary neutron star merger had far-reaching implications for our understanding of several open questions in physics and astrophysics. Unfortunately, since then, only one robust binary neutron star merger was detected through gravitational waves, GW190425, and no electromagnetic counterpart was identified for it. We analyze all reported electromagnetic followup observations of GW190425 and find that while the gravitational-wave localization uncertainty was large, most of the 90% probability region could have been covered within hours had the search been coordinated. Instead, more than 5 days after the merger, the uncoordinated search covered only 50% of the probability, with some areas observed over 100 times, and some never observed. We further show that, according to some models, it would have been possible to detect the GW190425 kilonova, despite the larger distance and higher component masses compared to GW170817. These results emphasize the importance of coordinating followup of gravitational-wave events, not only to avoid missing future kilonovae, but also to discover them early. Such coordination, which is especially important given the rarity of these events, can be achieved with the Treasure Map, a tool developed specifically for this purpose.

### 1. INTRODUCTION

Binary neutron star (BNS) mergers were predicted to produce both gravitational waves (GWs; Clark & Eardley 1977) and electromagnetic (EM) radiation. The latter was theorized to be emitted in the form of two types of transients: a short gamma-ray burst (GRB; Eichler et al. 1989), and longer-duration emission from the radioactive decay of heavy elements synthesized via the *r*-process in the ejecta (Li & Paczyński 1998). This transient has been nicknamed “macronova” (Kulkarni 2005) or “kilonova” (Metzger et al. 2010)<sup>1</sup>.

All three predictions were confirmed with the first discovery of a GW signal from a BNS merger, GW170817, detected and localized by the Advanced Large Interferometer Gravitational-wave Observatory (LIGO; LIGO Scientific Collaboration et al. 2015), and the Advanced Virgo detector (Acernese et al. 2014), during their second observation run (O2), on August 17, 2017 (Abbott et al. 2017a). The GW source was localized to a region of  $\sim 30 \text{ deg}^2$  at a distance of  $\sim 40 \text{ Mpc}$  and had a to-

tal binary mass of  $2.74^{+0.04}_{-0.01} M_{\odot}$  (Abbott et al. 2017a). A short GRB, GRB170817A, consistent with the GW localization, was detected  $\sim 2$  seconds after the GW-determined merger time (Abbott et al. 2017b) by the Fermi Gamma-ray Burst Monitor (Fermi-GBM; Meegan et al. 2009), and the International Gamma-Ray Astrophysics Laboratory (INTEGRAL; Winkler et al. 2003). An optical transient, AT 2017gfo, also consistent with the GW localization, was detected 11 hours later (Coulter et al. 2017a). Both EM transients were later confirmed to be physically associated with the BNS merger (Abbott et al. 2017).

Specifically, AT 2017gfo was consistent with kilonova predictions whereby at the coalescence of a BNS system,  $10^{-4} - 10^{-2} M_{\odot}$  of neutron-rich material are ejected at velocities of  $0.1 - 0.3c$  in the equatorial plane due to tidal effects (e.g. Rosswog et al. 1999; Hotokezaka et al. 2013). Additional mass was predicted to be ejected in the polar direction from the contact region at the time of the merger (e.g. Bauswein et al. 2013; Hotokezaka et al. 2013). Lanthanides formed in low electron-fraction material, such as the equatorial tidal ejecta, have a high opacity (Kasen et al. 2013; Tanaka & Hotokezaka 2013), making the light curve redder, fainter, and longer lived compared to low lanthanide ejecta (Barnes & Kasen 2013; Grossman et al. 2014), such as that from polar regions. The result, seen in AT 2017gfo, is a kilonova

Corresponding author: Ido Keinan  
idokeinan1@mail.tau.ac.il

<sup>1</sup> Hereafter we use the term “kilonova” rather than “macronova” because it has been more widely adopted by the community.

of at least two components: one blue and short-lived from the lanthanide-poor ejecta, and one red and longer-lived from the lanthanide-rich ejecta. For a review of this event, see for e.g. Nakar (2020) and Margutti & Chornock (2021).

GW170817 and its EM counterparts confirmed that BNS mergers are sites of  $r$ -process nucleosynthesis (e.g. Kasen et al. 2017), and confirmed the connection between short GRBs and BNS mergers. This event also demonstrated a novel method to constrain the Hubble constant (Abbott et al. 2017). However, many open questions regarding the properties of the kilonova emission remain, such as whether the source of the early blue emission is indeed a distinct lanthanide-poor ejecta component (other physical mechanisms were proposed, e.g. Kasliwal et al. 2017; Piro & Kollmeier 2018; Waxman et al. 2018). More BNS detections and multi-wavelength observations of their EM counterparts, especially during the first few hours (e.g. Arcavi 2018) are needed to answer these questions.

The second (and so far, last) robust GW detection of a BNS merger occurred at the start of the third GW-detector observing run (O3). GW190425 was discovered on April 25, 2019, at 08:18:05 UTC, at a distance of  $159_{-72}^{+69}$  Mpc and with a total binary mass of  $3.4_{-0.1}^{+0.3} M_{\odot}$  (Abbott et al. 2020). The event was detected only by a single LIGO detector, making its localization poorly constrained, with a  $10183 \text{ deg}^2$  90% uncertainty region initially (Ligo Scientific Collaboration & VIRGO Collaboration 2019a). This region shrank about one day later to  $7461 \text{ deg}^2$  (Ligo Scientific Collaboration & VIRGO Collaboration 2019b), but grew back to  $9881 \text{ deg}^2$  in the final localization published in the second GW Transient Catalog (GWTC-2; Abbott et al. 2021). The localization parameters are summarized in Table 1, and the localization maps are shown in Figure 1.

No coincident GRB was detected by the Fermi Large Area Telescope (Fermi-LAT; Atwood et al. 2009; Axelsson et al. 2019), the Swift Burst Alert Telescope (Swift/BAT; Gehrels et al. 2004; Sakamoto et al. 2019) nor by the Fermi-GBM (Fletcher et al. 2019). The International Gamma-Ray Astrophysics Laboratory (INTEGRAL; Winkler et al. 2003) reported a detection of a low significance signal, associated with a BNS merger (Pozanenko et al. 2020), but with no localization information to robustly tie it to GW190425 (Savchenko et al. 2019).

An extensive EM followup effort to find the kilonova associated with GW190425 began shortly after the initial alert. However, no significant kilonova candidate was identified. This was attributed to the larger dis-

**Table 1.** GW190425 localization areas and distances.

Epoch	Date [UTC]	90% Area [ $\text{deg}^2$ ]	50% Area [ $\text{deg}^2$ ]	Distance [Mpc]
Initial	2019-04-25	10183	2806	$154 \pm 45$
Alert	08:19:27			
Update	2019-04-26	7461	1378	$156 \pm 41$
Alert	10:48:17			
GWTC-2	2020-07-27	9881	2400	$157 \pm 43$
	16:41:49			

NOTE—“90% (50%) Area” refers to the sky area that contains 90% (50%) of the probability for the location of the source.

tance, higher component masses, more equal mass ratio, and to the larger localization compared to GW170817 (e.g. Hosseinzadeh et al. 2019a; Lundquist et al. 2019; Abbott et al. 2020; Foley et al. 2020; Gompertz et al. 2020; Kyutoku et al. 2020; Sagués Carracedo et al. 2021; Camilletti et al. 2022; Dudi et al. 2022; Radice et al. 2024). However, here we show that, according to some models, the emission from the GW190425 kilonova could have been detected by existing facilities, and that most of the localization could have been covered within hours, had the EM followup effort been coordinated.

Coordinating EM followup of GW events is challenging. Reports of observations and possible kilonova candidates during O2 and O3 were primarily communicated through GRB Coordinates Network<sup>2</sup> (GCN; now the General Coordinates Network) circulars. GCN circulars were designed to be human readable, with no unified text format. As such they are not ideal when reporting lists of coordinates, bands, and sensitivities observed. The non machine-readable format makes it very difficult to parse, store and interpret such information in real time.

One tool designed to address the challenge of coordinating EM followup of GW events is the **Treasure Map**<sup>3</sup> (Wyatt et al. 2020). **Treasure Map** is a web application that collects, stores and distributes followup reports through a machine-friendly Application Programming Interface (API). The API allows observers to report their planned and executed observations and to retrieve those of other facilities in order to inform their own counterpart search plan in real time. In addition, an interactive visualization allows observers to see their

<sup>2</sup> <https://gcn.nasa.gov/>

<sup>3</sup> <https://treasuremap.space/>

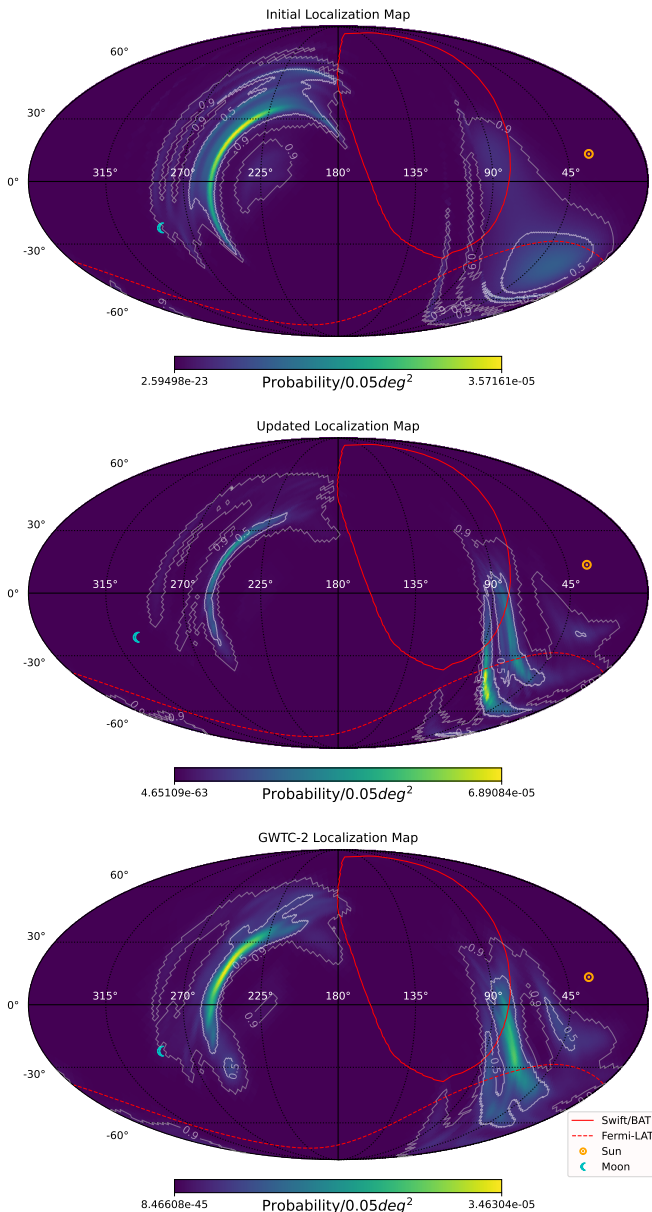


**Figure 1.** GW190425 localizations released in the initial (top) and update (middle) alerts, and in the final GWTC-2 publication (bottom; Abbott et al. 2021). White and grey contours denote the regions containing 50% and 90% of the probability of the source location, respectively. The Swift/Bat and Fermi-LAT footprints at the time of the merger are presented in red solid and dashed lines, covering areas of  $4596 \text{ deg}^2$  and  $8602 \text{ deg}^2$ , respectively. The position of the Sun and Moon at the time of the merger are denoted in their respective symbols.

observations and those of other facilities on a map, together with GW localization in an intuitive way. All of the reports are also available to download at a later date for analyzing followup efforts and non-detection statistics. Unfortunately, the *Treasure Map* did not exist

during GW190425, leading to very inefficient followup, as we will show here. Our goal is to encourage the community to use tools such as the *Treasure Map* during the next BNS merger, in order to increase the chances of finding the EM counterpart, and to do so as quickly as possible. We do so by demonstrating the impact of uncoordinated observations on missing the counterpart to GW190425.

In this work, we analyze all reported infrared, optical and ultraviolet followup efforts of GW190425. In Section 2 we describe our data sources and collection process; in Section 3, we analyze the sky coverage and depth achieved in the context of the expected kilonova emission from this event; and, finally, in Section 4, we discuss our conclusions.

## 2. DATA

In order to analyze the efficiency of the search for the GW190425 EM counterpart we collected pointing and photometric data of infrared, optical and ultraviolet observations obtained as followup of GW190425 up to 2019 April 30, 23:57:21 UTC, which were reported in one of the following sources (removing duplicate reports of the same observations): The *Treasure Map* (1419 observations reported retroactively), 122 GCN circulars (1339 observations), the MASTER global robotic net (MASTER-Net; Lipunov et al. 2010) website<sup>4</sup> (4491 observations), the Coulter et al. (2024) report on the One-meter Two-hemispheres (1M2H) followup (345 observations), the Smartt et al. (2024) report of the Panoramic Survey Telescope and Rapid Response System (Pan-STARRS) and the Asteroid Terrestrial-impact Last Alert System (ATLAS) followup (232 and 422 observations, respectively), and the Becerra et al. (2021) report (augmented with R.L. Becerra, private communication) of the Deca-Degree Optical Transient Imager (DDOTI) followup (10 observations).

In total, 8258 unique observations were collected, including time stamps and bands used. Limiting magnitudes are available for all except for the pointings of the Corrector de Óptica Activa y de Tilts al Límite de Difracción (COATLI; Watson et al. 2019), the Korea Microlensing Telescope Network (KMTNet; Kim et al. 2019) and Pan-STARRS in the  $z$ -band, which we include here for coverage analysis only. Instrument footprints and fields of view (FOVs) for all pointings analyzed here were taken from the *Treasure Map* when available, from GCN reports when provided there, and from instrument-specific websites and publications oth-

<sup>4</sup> <http://observ.pereplet.ru/>

erwise (all references are provided in Table 2). Some galaxy-targeted searches provided target galaxy names rather than exact coordinates pointed to. In such cases, we obtained the galaxy coordinates from the Galaxy List for the Advanced Detector Era (GLADE) catalog (Dályá et al. 2018) or the SIMBAD Astronomical Database

(Wenger et al. 2000) and assumed the target galaxies were positioned at the center of the observed footprint. A summary of the observations and instruments used in this analysis is presented in Table 2, and the full list of all pointings gathered is presented in Table 3.

**Table 2.** GW190425 EM followup observations reported in circulars, the **Treasure Map**, by MASTER-Net on their website, and in Coulter et al. (2024), Smartt et al. (2024) and Becerra et al. (2021), out to 5.65 days after merger.

Group/Facility/Instrument	No. of Pointings	Bands	Field of View [deg <sup>2</sup> ]	Median 5 $\sigma$ Depth [AB Mag]	Pointings Reference
MASTER-Net <sup>a</sup>	4491	Clear	8.00	19.10	1
ZTF <sup>b</sup>	596	g,r,i	46.73	21.05	2
ATLAS <sup>c</sup>	422	o,c	28.89	19.26	3
Swift/UVOT <sup>d</sup>	392	u	8.0e-02	19.40	2
GOTO <sup>e</sup>	303	V,g	18.85	19.85	2
Pan-STARRS <sup>f</sup>	232	w,i,z	7.06	21.58	3
J-GEM/Subaru <sup>g</sup>	154	r	2.0e-03	24.00	4
1M2H/Swope <sup>h</sup>	151	B,V,u,g,r,i	0.25	21.55	5
COATLI <sup>i</sup>	128	w	3.3e-02	n/a	6
KMTNet 1.6m <sup>j</sup>	120	R	4.00	n/a	7
KAIT <sup>k</sup>	101	Clear	1.2e-02	19.00	8
Harold Johnson Telescope/RATIR <sup>l</sup>	99	J,H,Y,Z,g,r,i	8.1e-03	20.74	9, 10
GROWTH/LOT <sup>m</sup>	93	R,g,r,i	3.6e-02	19.79	11, 12, 13
1M2H/Nickel <sup>n</sup>	93	r,i	1.1e-02	20.24	5
MMTO/MMTCam <sup>o</sup>	81	g,i	2.0e-03	21.48	2, 14
GWAC-F60A <sup>p</sup>	80	Clear	9.0e-02	18.97	15
CNEOST <sup>q</sup>	75	R	9.00	19.86	16
BOOTES-5 <sup>r</sup>	63	Clear	2.78	20.50	17
SAGUARO/CSS 1.5m <sup>s</sup>	61	Clear	5.00	21.30	2
LCO 1m <sup>t</sup>	58	g,r,i	0.20	21.30	18, 19, 20, 21
1M2H/Thacher <sup>u</sup>	53	g,r,z	0.12	19.55	5
GRANDMA/LesMakes T60 <sup>v</sup>	52	Clear	17.64	19.20	22
GRANDMA/AZT-8 <sup>w</sup>	52	B,R	0.25	19.00	22
GRANDMA/Abastumani T70 <sup>x</sup>	40	R	0.25	16.29	22
Xinglong 60/90cm <sup>y</sup>	35	Clear	2.25	18.00	23
McDonald Observatory 2.1m/CQUEAN <sup>z</sup>	30	i	6.1e-03	20.44	24
1M2H/ANDICAM-CCD <sup>aa</sup>	27	I	1.1e-02	20.70	5
GROWTH/Kitt Peak 2.1m/KPED <sup>ab</sup>	25	I,g,r	7.0e-03	20.40	25, 26, 27
YAHPT <sup>ac</sup>	23	R	3.4e-02	18.18	28
1M2H/ANDICAM-IR <sup>ad</sup>	21	J,H,K	1.5e-03	13.45	5
Liverpool Telescope/IO:O <sup>ae</sup>	19	g,r,i,z	2.8e-02	22.24	29, 30
LOAO 1m <sup>af</sup>	13	R	0.22	19.23	31

**Table 2** continued

**Table 2** (*continued*)

Group/Facility/Instrument	No. of Pointings	Bands	Field of View [deg <sup>2</sup> ]	Median 5 $\sigma$ Depth [AB Mag]	Pointings Reference
GROWTH-India <sup>ag</sup>	10	g,r,i	0.49	18.41	32, 33
Konkoly 0.8m <sup>ah</sup>	10	g,r	9.0e-02	20.40	34
DDOTI <sup>ai</sup>	10	w	11.56	19.95	35
IRSF 1.4m/SIRIUS <sup>aj</sup>	7	J,H,K	1.6e-02	15.31	36, 37
TAROT TRE <sup>ak</sup>	7	R	17.64	17.23	38
Konkoly 0.6/0.9m <sup>al</sup>	5	Clear	1.36	21.50	34
Lijiang 2.4m <sup>am</sup>	5	g,r	2.56	19.04	39
GRANDMA/CAHA 2.2m <sup>an</sup>	5	U,B,V,R,I	4.5e-02	22.30	40
DECam <sup>ao</sup>	4	g,r,i,z	3.35	23.85	41
MPG/GROND <sup>ap</sup>	3	r,i,z	8.1e-03	20.00	42
NOT/ALFOSC <sup>aq</sup>	3	g,r,i	1.1e-02	20.39	43
OSN 1.5m <sup>ar</sup>	2	R	6.8e-02	21.30	44, 45
ANU/SkyMapper <sup>as</sup>	2	i	5.62	20.00	46
GTC/OSIRIS <sup>at</sup>	1	r	1.8e-02	22.80	45
VISTA/VIRCAM <sup>au</sup>	1	K	2.14	19.55	47

**Table 2** *continued*

Table 2 (continued)

Group/Facility/Instrument	No. of Pointings	Bands	Field of View [deg <sup>2</sup> ]	Median 5 $\sigma$ Depth [AB Mag]	Pointings Reference
---------------------------	---------------------	-------	--------------------------------------	-------------------------------------	---------------------

NOTE—Sources which did not provide their observation depths are marked with “n/a” in the depth column. The median depth for Pan-STARRS is for the  $w$  and  $i$  bands, as no observation depths were provided for the  $z$ -band.

Instrument references: <sup>a</sup>Mobile Astronomical System of TElescope Robots (Lipunov et al. 2010); <sup>b</sup>Zwicky Transient Facility (Masci et al. 2018); <sup>c</sup>Asteroid Terrestrial-impact Last Alert System (Tonry et al. 2018) <sup>d</sup>Swift Ultraviolet/Optical Telescope (Roming et al. 2005); <sup>e</sup>Gravitational-wave Optical Transient Observer (Dyer et al. 2022); <sup>f</sup>Panoramic Survey Telescope and Rapid Response System (Chambers et al. 2016) <sup>g</sup>Japanese Collaboration for Gravitational-wave ElectroMagnetic followup (Yoshida et al. 2000; Kashikawa et al. 2002); <sup>h</sup>One-Meter Two-Hemispheres/Swope (Bowen & Vaughan 1973); <sup>i</sup>Corrector de Óptica Activa y de Tilts al Límite de dIfracción (Watson et al. 2016a); <sup>j</sup>Korea Microlensing Telescope Network (Kim et al. 2016); <sup>k</sup>Katzman Automatic Imaging Telescope (Filippenko et al. 2001); <sup>l</sup>Reionization and Transients Infrared Camera (Farah et al. 2010); <sup>m</sup>Global Relay of Observatories Watching Transients Happen/Lulin One-meter Telescope (Kasliwal et al. 2019); <sup>n</sup>Nickel Direct Imaging Camera ([https://mthamilton.ucolick.org/techdocs/instruments/nickel\\_direct/intro/](https://mthamilton.ucolick.org/techdocs/instruments/nickel_direct/intro/)); <sup>o</sup>MMT Observatory (Fabricant et al. 2019); <sup>p</sup>Ground Wide Angle Cameras Array (Han et al. 2021); <sup>q</sup>Chinese Near Earth Object Survey Telescope; <sup>r</sup>Burst Observer and Optical Transient Exploring System 5; <sup>s</sup>Searches After Gravitational-waves Using ARizona’s Observatories/Catalina Sky Survey (Drake et al. 2009); <sup>t</sup>Las Cumbres Observatory (Brown et al. 2013); <sup>u</sup>Thacher ACP Camera Swift et al. (2022); <sup>v</sup>Global Rapid Advanced Network Devoted to the Multi-messenger Addicts (Antier et al. 2020); <sup>w</sup>Astronomical Reflecting Telescope 8 (Antier et al. 2020); <sup>x</sup>Abastumani(Antier et al. 2020); <sup>y</sup>Xinglong 60/90cm, Chinese Academy of Sciences; <sup>z</sup>Camera for QUasars in EARly uNiverse (Park et al. 2012); <sup>aa</sup>A Novel Dual Imaging CAMera (ANDICAM) CCD (DePoy et al. 2003); <sup>ab</sup>Kitt Peak EMCCD Demonstrator; <sup>ac</sup>YAoan High Precision Telescope (Guo et al. 2022); <sup>ad</sup>ANDICAM-IR (DePoy et al. 2003); <sup>ae</sup>Infrared-Optical:Optical (Steele et al. 2004); <sup>af</sup>Lemmonsan Optical Astronomy Observatory (Han et al. 2005); <sup>ag</sup>Kasliwal et al. (2019); <sup>ah</sup>Konkoly 0.8m Telescope, Research Centre for Astronomy and Earth Sciences; <sup>ai</sup>Deca-Degree Optical Transient Imager (Watson et al. 2016b); <sup>aj</sup>InfraRed Survey Facility/Simultaneous InfraRed Imager for Unbiased Survey (Nagayama et al. 2003); <sup>ak</sup>Télescope à Action Rapide pour les Objets Transitoires (Boër et al. 1999); <sup>al</sup> Konkoly 0.6/0.9m (<https://old.konkoly.hu/konkoly/telescopes.html>); <sup>am</sup>(Wang et al. 2019); <sup>an</sup>Centro Astronómico Hispano en Andalucía (Antier et al. 2020); <sup>ao</sup>Dark Energy Camera (Flaugher et al. 2015); <sup>ap</sup>Max Planck Gesellschaft/Gamma-Ray burst Optical and Near-infrared Detector (Greiner et al. 2008); <sup>aq</sup>Nordic Optical Telescope/ALhambra Faint Object Spectrograph and Camera (Djupvik & Andersen 2010); <sup>ar</sup>Observatorio de Sierra Nevada (<https://www.osn.iaa.csic.es/en/page/15-m-telescope>); <sup>as</sup>Australian National University (Keller et al. 2007); <sup>at</sup>Gran Telescopio Canarias/Optical System for Imaging and low-intermediate Resolution Integrated Spectroscopy (Cobos et al. 2002); <sup>au</sup>Visible and Infrared Survey Telescope for Astronomy/VISTA InfraRed CAMera (Emerson et al. 2006; Dalton et al. 2006).

Pointings references: <sup>1</sup><https://observ.pereplet.ru/> (Lipunov et al. 2010); <sup>2</sup><https://treasuremap.space/> (Wyatt et al. 2020); <sup>3</sup>Smartt et al. (2024); <sup>4</sup>Sasada et al. (2019); <sup>5</sup>Coulter et al. (2024); <sup>6</sup>Watson et al. (2019); <sup>7</sup>Kim et al. (2019); <sup>8</sup>Zheng et al. (2019); <sup>9</sup>Butler et al. (2019); <sup>10</sup>Troja et al. (2019); <sup>11</sup>Tan et al. (2019a); <sup>12</sup>Tan et al. (2019b); <sup>13</sup>Kong (2019); <sup>14</sup>Hosseinzadeh et al. (2019b); <sup>15</sup>Xin et al. (2019); <sup>16</sup>Li et al. (2019a); <sup>17</sup>Hu et al. (2019a); <sup>18</sup>Burke et al. (2019); <sup>19</sup>Hiramatsu et al. (2019a); <sup>20</sup>Hiramatsu et al. (2019b); <sup>21</sup>Arcavi et al. (2019); <sup>22</sup>Howell et al. (2019); <sup>23</sup>Xu et al. (2019); <sup>24</sup>Im et al. (2019); <sup>25</sup>Ahumada et al. (2019b); <sup>26</sup>Ahumada et al. (2019a); <sup>27</sup>Ahumada et al. (2019c); <sup>28</sup>Sun et al. (2019); <sup>29</sup>Perley & Copperwheat (2019); <sup>30</sup>Perley et al. (2019); <sup>31</sup>Paek et al. (2019); <sup>32</sup>Bhalerao et al. (2019); <sup>33</sup>Waratkar et al. (2019); <sup>34</sup>Vinko et al. (2019); <sup>35</sup>Becerra et al. (2021), R. L. Becerra, private communication; <sup>36</sup>Morihana et al. (2019a); <sup>37</sup>Morihana et al. (2019b); <sup>38</sup>Blazek et al. (2019); <sup>39</sup>Li et al. (2019b); <sup>40</sup>Kann et al. (2019); <sup>41</sup>Bloom et al. (2019); <sup>42</sup>Schady et al. (2019); <sup>43</sup>Izzo et al. (2019); <sup>44</sup>Castro-Tirado et al. (2019); <sup>45</sup>Hu et al. (2019b); <sup>46</sup>Chang et al. (2019); <sup>47</sup>Tanvir et al. (2019).

### 3. ANALYSIS AND RESULTS

In order to measure the efficiency of the search for the GW190425 EM counterpart, we first analyze the observability of the GW localization region at the time of the merger (Section 3.1), followed by the amount of the GW localization that was covered as a function of time, in

terms of the total probability, area, and galaxy luminosity (Sections 3.2 and 3.3). We then examine the reported non-detection limiting magnitudes and compare them to light curves of the GW170817 kilonova and of kilonova models tuned to the parameters of GW190425 (Section 3.4).

GW localizations are provided as Hierarchical Equal Area isoLatitude Pixelation<sup>5</sup> (HEALPix; Górski et al.

<sup>5</sup> <https://HEALPix.sourceforge.io/>

**Table 3.** List of the observations used in this work.

Facility/Instrument	MJD	R.A. [deg]	Dec. [deg]	Band	$5\sigma$ Limiting Mag.	Source
ZTF	58598.3460	180.0000	62.1500	r	20.46	Treasure Map
ZTF	58598.3465	-168.6100	54.9500	r	20.95	Treasure Map
ZTF	58598.3470	-165.0502	47.7500	r	21.05	Treasure Map
ZTF	58598.3474	-167.7500	40.5500	r	20.80	Treasure Map

NOTE—This table is published in its entirety in the machine readable format. A portion is shown here for guidance regarding its form and content.

2005) maps. These maps divide the sky into pixels of equal area and assign a probability value for the location of the GW source to each pixel. Each pixel is also assigned a distance to the source (assuming it is at that position) and a distance error estimate. The number of pixels  $N_{pixels}$  in the map is  $12 \cdot (n_{side})^2$  with  $n_{side} = 2^n$  for some integer  $n \geq 0$ . The localization maps provided for GW190425 have a resolution of  $n_{side} = 256$ , or  $N_{pixels} = 786432$ . This translates into pixels with an area of  $0.052 \text{ deg}^2$  each. We perform all of our analysis using the maps in this resolution, as they were provided, except for the observability analysis (Section 3.1), for which we downsample the maps to  $n_{side} = 32$  (i.e.  $N_{pixels} = 12288$  and a pixel area of  $3.36 \text{ deg}^2$ ) for computational ease.

### 3.1. Observability

We define that a region on the sky is “visible” at a point in time from a certain location on Earth when the Sun is at least  $12^\circ$  below the horizon, the Moon separation is at least  $20^\circ$  (the moon illumination was 66% at the time of the GW190425 merger) and the airmass is less than 2.5. According to this definition, of the  $9881 \text{ deg}^2$  ( $2400 \text{ deg}^2$ ) of the 90% (50%) final localization,  $7783 \text{ deg}^2$  ( $2182 \text{ deg}^2$ ), or roughly 79% (91%), were visible during the 24 hours following the merger from the combined locations of all ground-based observatories listed in Table 2.

Next, we define the “accessibility” of each area of the sky to each instrument as the amount of time per day that area is visible to that instrument,  $t_{visible}$ , weighted by the instrument FOV (to take into account that larger FOV instruments can cover more area simultaneously) and divided by the pixel area of the map ( $3.36 \text{ deg}^2$  in this case):

$$t_{accessibility} = t_{visible} \left( \frac{FOV}{3.36 \text{ deg}^2} \right) \quad (1)$$

We define an inaccessible area as one with total accessibility (i.e. summed over all ground-based instruments

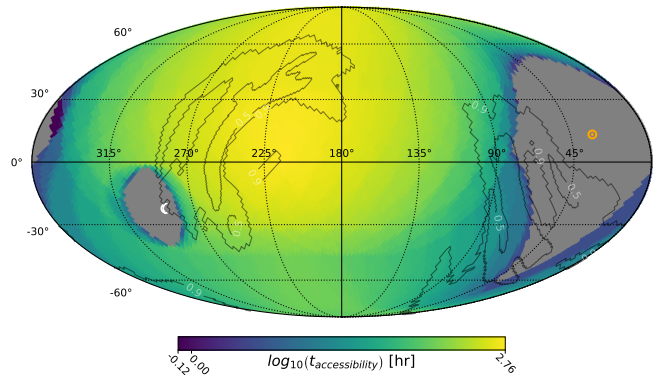


**Figure 2.** Accessible hours during the first day after the merger summed over all ground-based observatories listed in Table 2. An accessible hour is one that is over an airmass of 2.5 and not sun or moon-constrained, normalized to the FOV of each instrument (see text for details). Grey regions indicate inaccessible areas ( $t_{accessibility} < 5 \text{ min}$ ). Black contours are of the GWTC-2 localization. The sun and moon locations in the figure at the time of the merger.

considered here)  $t_{accessibility} < 5 \text{ min}$  (corresponding to a typical single exposure time). Using this definition,  $6284 \text{ deg}^2$  of the sky were inaccessible due to sun and moon constraints, of which  $2098 \text{ deg}^2$  were in the GWTC-2 90% localization region. The rest of the localization region, encompassing 75% of the probability, was visible with a median total accessibility time of 41.5 hours. The total accessibility of the 90% localization region during the first day since merger is presented in Figures 2 and 3, and in Table 4.

### 3.2. Area and Probability Coverage

We count the sky area and the probability observed up to 5.65 days after the time of the merger, both with and without overlap between observations, in order to measure how much of the localization was covered and how much of it was observed multiple times. Measuring total area and probability on a HEALPix map requires

**Table 4.** GW190425 accessible localization areas and probabilities, and median accessibility.

Epoch	90% Area [ $deg^2$ ]	Accessible 90% Area [ $deg^2$ ]	Accessible Probability	Median Accessibility [Hr]
Initial	10183	8216	72%	80.0
Update	7461	5833	76%	32.0
GWTC-2	9881	7783	75%	41.5

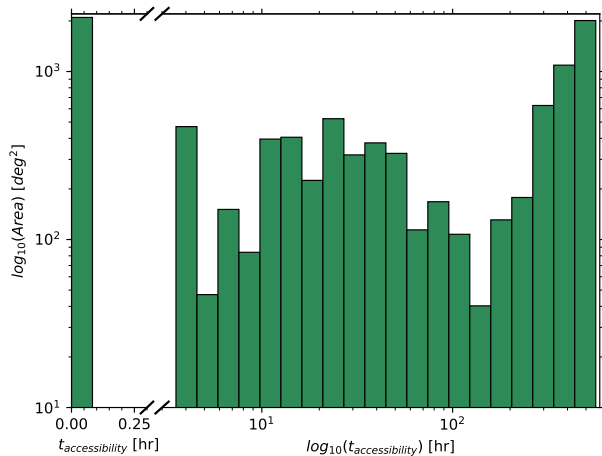


**Figure 3.** Accessible hours of the GWTC-2 90% localization during the first day after merger. Out of the 90% localization area, 2098  $deg^2$  were inaccessible ( $t_{accessibility} < 5$  min, leftmost bin), leaving 75% of the probability accessible, with a median total accessibility of 41.5 hours.

counting the pixels that overlap with an observed footprint. Due to the resolution of the map, the minimal area that can be counted per footprint is  $0.052 deg^2$ . However, there are footprints with a smaller FOV (as seen in Table 2). Here we use the `healpy`<sup>6</sup> python package, which includes two methods for counting (“querying”) pixels inside an observed footprint. The “inclusive” method counts every pixel that overlaps with the footprint, while the “exclusive” method only counts pixels that have their center fall inside the footprint. An illustration of these two methods is presented in Figure 8 in Appendix A. We choose the exclusive method for our analysis, as it is a more conservative accounting of the actual area and probability covered, while the inclusive

<sup>6</sup> <https://healpy.readthedocs.io/>

method over counts pixels, causing an overestimation of the area and probability covered.

Figure 4 shows the total coverage of all reported followup observations up to 5.65 days post-merger outlined in Section 2. Some regions, in the northern part of the localization, were observed more than 100 times while most of the accessible southern part of the localization was not observed at all.

The GW localization was updated 26 hours after the initial localization was released. At the time of the update, earlier footprints had their probability coverage changed. We take that into account by retroactively recounting the probability covered by all of the observations using the updated localization from the time it was released. The area covered does not depend on the localization map and thus, no recounting of the area covered is needed at the time of the update. The sum of area and probability covered is performed in two different ways, first without regard to whether observations overlap or not, and second with overlapping regions counted only once. We compare the probability covered to the 100% probability of the entire sky and the area covered to the initial and updated 90% probability areas.

The probability and area covered as a function of time are shown in Figure 5. Within 5.65 days following the merger, 11486  $deg^2$  were covered (once or more). This is more than the area of the GWTC-2 90% probability region, but not all of the area covered is in that region (Fig. 4). In fact, at 5.65 days post-merger, only 54% of the probability (of the GWTC-2 localization) was covered, while enough observations were made to cover over 120000  $deg^2$  by that time. According to Figure 5, an area equivalent to the 90% probability region was covered within three hours from merger. This means that ideally coordinated observations could have covered the accessible 90% localization within hours<sup>7</sup>.

### 3.3. Galaxy Luminosity Coverage

We define the galaxy luminosity coverage as the fraction of  $B$ -band luminosity of galaxies observed out of the total  $B$ -band luminosity of all galaxies with  $L > L_B^*$  in the 90% localization volume within  $3\sigma$  of the mean localization distance. Here,  $L_B^*$  is the  $B$ -band luminosity corresponding to  $L^*$ , the characteristic luminosity of the Schechter Function (Schechter 1976). We adopt a corresponding absolute magnitude in the  $B$  band of  $M_B^* = -20.7$ , following Arcavi et al. (2017a). The

<sup>7</sup> Instrument-specific observability constraints could prolong this time estimate, but we consider this a simple order-of-magnitude estimate of the time it would have taken to cover the region under ideal conditions.



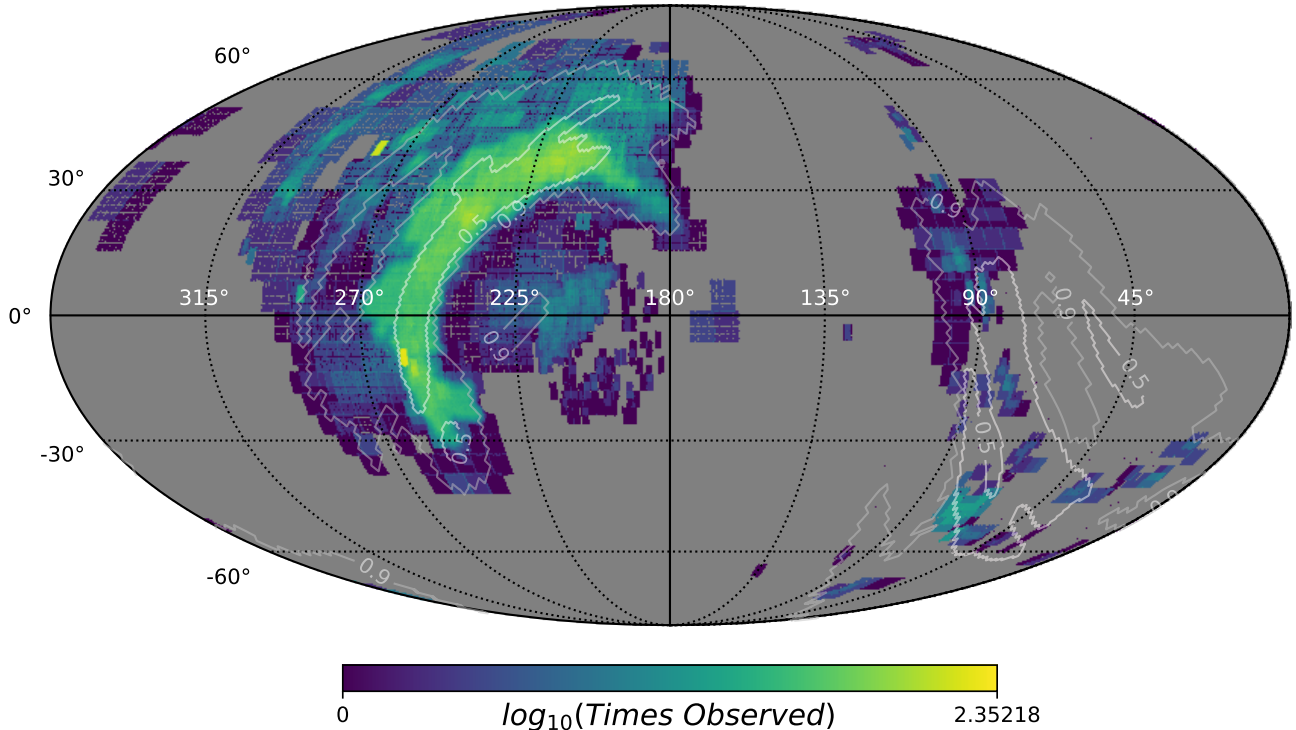


**Figure 4.** Total number of infrared, optical and ultraviolet followup observations up to 5.65 days post merger for GW190425. Grey areas are where no observations were reported. Lines mark the 50% and 90% probability regions of the final GWTC-2 localization. While some parts of the localization were observed over 100 times, some were not observed at all, even though they were accessible (Figure 2).

GLADE catalog is less complete to galaxies fainter than  $L^*$  at large distances (see Dálya et al. 2018, for more details).

We count only galaxies that have a  $B$ -band apparent magnitude and a distance estimate in Version 2.3 of the GLADE catalog. There are a total of 47664 (34302) such galaxies in the catalog inside the initial (updated) 90% localization.

We count galaxies that are inside observed footprints and the localization volume, once with recounting galaxies and once without. Figure 6 shows the galaxy luminosity coverage as a function of time. After 5.65 days from the merger, only 52% of the  $B$ -band luminosity in galaxies inside the updated localization region was observed, while 11.88 times the localization luminosity was observed in total due to overlapping observations.

### 3.4. Kilonova Detection

Even if the localization would have been covered as efficiently as possible, there is still a possibility that the EM counterpart was too faint to have been detected.

In order to check this, we compare the non-detection limiting magnitudes reported for each of the followup observations to the light curve of GW170817 and to light curves generated using the Kasen et al. (2017) and Nicholl et al. (2021) kilonova models.

We use the InfraRed Survey Archive (IRSA) dust extinction service queries<sup>8</sup> to correct all reported magnitude limits for Milky Way dust extinction at the center of their footprint by using the Schlafly & Finkbeiner (2011) galactic dust extinction estimates. For unfiltered observations, we assume  $r$ -band extinction. We then translate all limits to absolute magnitudes using the mean distance of the pixel that overlaps with the footprint center.

The GW170817 data is taken from the Arcavi (2018) compilation of observations by Andreoni et al. (2017); Arcavi et al. (2017b); Coulter et al. (2017b); Cowperthwaite et al. (2017); Díaz et al. (2017); Drout et al. (2017); Evans et al. (2017); Hu et al. (2017); Kasliwal et al.

<sup>8</sup> [https://astroquery.readthedocs.io/en/latest/ipac/irsa/irsa\\_dust/irsa\\_dust.html](https://astroquery.readthedocs.io/en/latest/ipac/irsa/irsa_dust/irsa_dust.html)

**Table 5.** Parameters and distributions used for generating the ensemble of light curves from the Nicholl et al. (2021) BNS merger kilonova model.

Parameter	Description	Type	Values
$\mathcal{M}^a$ [ $M_\odot$ ]	Chirp mass	Gaussian	$\mu = 1.44, \sigma = 0.02$
$q^a$	Mass ratio (high spin case)	uniform	min = 0.4, max = 1.0
	Mass ratio (low spin case)	uniform	min = 0.8, max = 1.0
s	Shock density profile power law index	fixed	1.0
$M_{TOV}$ [ $M_\odot$ ]	NS maximum theoretical mass	fixed	2.2
$\alpha^b$	Enhancement of blue ejecta	fixed	1.0
$disk_{frac}^b$	Fraction of disk ejected	fixed	0.15
$\cos \theta^b$	Cosine of viewing angle	uniform	min = 0.0, max = 1.0
$\cos \theta_{cocoon}^b$	Cosine of cocoon opening angle	uniform	min = 0.707, max = 1.0
$\cos \theta_{open}^b$	Cosine of squeezed ejecta opening angle	uniform	min = 0.707, max = 1.0
$\log N_H^b$	Hydrogen column density	uniform	min = 19, max = 23

<sup>a</sup>Based on the inferred values in Abbott et al. (2020) for the cases of high and Low spin.

<sup>b</sup>Based on the priors used in Nicholl et al. (2021).

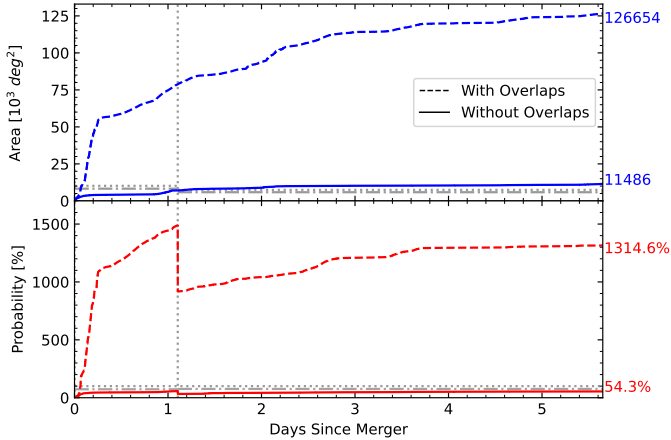


**Figure 5.** Cumulative area (top) and probability (bottom) observed during the 5.65 days following the GW190425 merger. Colored dashed lines are for all observations (including overlapping ones) while solid lines are for unique positions on the sky (without overlap). Horizontal grey dotted lines denote the total area inside the 90% localization region and 100% probability reported at the time, for the top and bottom plots, respectively, while the grey dash-dotted lines are for the accessible area and probability (see Section 3.1). The vertical grey dotted line denotes the time of the updated localization.

(2017); Lipunov et al. (2017); Pian et al. (2017); Shappee et al. (2017); Smartt et al. (2017); Tanvir et al. (2017); Troja et al. (2017); Utsumi et al. (2017); Valenti et al. (2017) and Pozanenko et al. (2018).

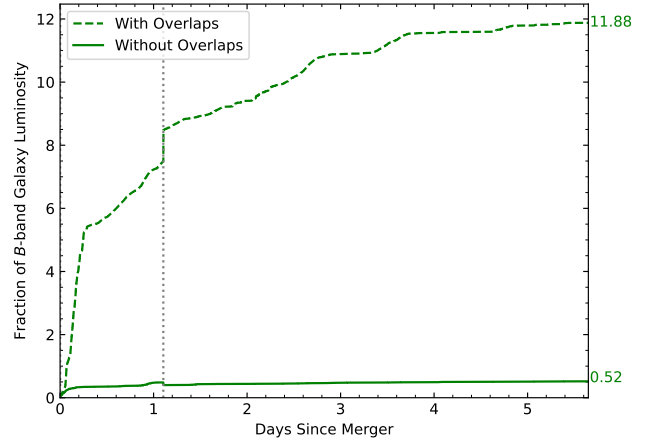


**Figure 6.**  $B$ -band Galaxy luminosity fraction observed out of all galaxies with luminosity larger than  $L_B^*$  from the GLADE 2.3 catalog that are inside the 90% localization region and up to a distance of  $3\sigma$  of the mean estimated distance. The initial and updated localizations are separated by the vertical dotted grey line. The dashed line shows the total luminosity observed including overlapping galaxies, while the solid line shows the total luminosity observed in unique galaxies.

The Kasen et al. (2017) model is based on a 1D Monte Carlo simulation of the radiative transfer of photons from the radioactive decay of  $r$ -process elements through kilonova ejecta. The ejecta is modeled using three parameters: ejecta mass  $M_{ej}$ , characteristic expansion ve-

**Table 6.** Ejecta parameters for two Kasen et al. (2017) models with lanthanide fractions  $X_{lan} = -2$  and  $X_{lan} = -4$ , and two Nicholl et al. (2021) models (low and high spin cases) with the priors from Table 5.

Model	$M_{ej} [M_{\odot}]$	$v_k [c]$	$\kappa_{ej} [cm^2/g]$
Kasen et al. (2017) <sup>a</sup>			
$X_{lan} = -2$	0.04	0.15	1
$X_{lan} = -4$	0.04	0.10	10
Nicholl et al. (2021) High-spin <sup>b</sup>			
Blue Component	$0.00065 \pm 0.00013$	$0.1550 \pm 0.0022$	0.5
Red Component	$0.0408 \pm 0.0044$	$0.552 \pm 0.0019$	10
Purple Component	$0.00565 \pm 0.00058$	$0.0505 \pm 0.0010$	$\simeq 5.6$
Total/Mean	$0.0471 \pm 0.0040$	$0.1973 \pm 0.0068$	$\simeq 8.4$
Nicholl et al. (2021) Low-spin <sup>b</sup>			
Blue Component	$0.00223 \pm 0.00013$	$0.1666 \pm 0.0012$	0.5
Red Component	$0.00401 \pm 0.00028$	$0.2420 \pm 0.0007$	10
Purple Component	$0.01120 \pm 0.00051$	$0.0578 \pm 0.0003$	$\simeq 5.55$
Total/Mean	$0.01740 \pm 0.00053$	$0.1186 \pm 0.0023$	$\simeq 5.87$

<sup>a</sup>Taken from [https://github.com/dnkasen/Kasen\\_Kilonova\\_Models\\_2017](https://github.com/dnkasen/Kasen_Kilonova_Models_2017) and Kasen et al. (2017).

<sup>b</sup>Calculated from binary parameters based on <https://github.com/mnicholl/kn-models-nicholl2021>.

locity  $v_k$ , and lanthanide fraction power index  $X_{lan}$  (where the lanthanide fraction is  $10^{X_{lan}}$ ). The calculation produces a spectral energy distribution of the emission. We use `pyphot`<sup>9</sup> to create synthetic light curves in the relevant bands from these model spectra. We use the ejecta parameters assumed by Foley et al. (2020) for the GW190415 kilonova:  $M_{ej} = 0.04M_{\odot}$ ,  $v_k = 0.15c$  and  $X_{lan} = -2$ , which they propose assuming a BNS system with masses  $1.4M_{\odot}$  and  $2.0M_{\odot}$ . This lanthanide fraction results in a high opacity of  $\kappa_{ej} \approx 10 \text{ cm}^2/g$  and a transient that is observable mostly in the infrared. This led Foley et al. (2020) to conclude that the GW190425 kilonova would not have likely been observable to most facilities that participated in the search. To illustrate the effect of the assumed lanthanide fraction we also use a model with  $M_{ej} = 0.04M_{\odot}$ ,  $v_k = 0.10c$  and  $X_{lan} = -4$ . The lower lanthanide fraction compared to the Foley et al. (2020) parameters results in a lower opacity of  $\kappa_{ej} \approx 1 \text{ cm}^2/g$ , leading to a bluer and brighter kilonova.

Nicholl et al. (2021) provide an analytic 2D kilonova model that assumes a three-component ejecta: one component is the “tidal ejecta” in the equatorial region and

a second is the “polar ejecta” concentrated in the polar region. For both components, a blackbody is assumed. The third component is from GRB-shocked material in a “cocoon” around the polar region (Nakar & Piran 2016). The model parameters relate directly to the GW-measured binary system chirp mass  $\mathcal{M}$  and mass ratio  $q$ , and to neutron star (NS) equation of state parameters, such as the NS maximum theoretical mass  $M_{TOV}$ . These are used to calculate the mass  $M_{ej}$ , velocity  $v_k$ , and the opacity  $\kappa_{ej}$  of each ejecta component corresponding to three opacity regimes: the “red” high opacity (low  $Y_e$ ) tidal ejecta, the “blue” low opacity (high  $Y_e$ ) polar ejecta, and the intermediate-opacity “purple” ejecta. The blue and red opacities are assumed to be  $\kappa_{ej,blue} = 0.5 \text{ cm}^2/g$  and  $\kappa_{ej,red} = 10 \text{ cm}^2/g$ , respectively. The asymmetry of the ejecta is parameterized by the opening angle around the poles  $\theta_{open}$ , which separates the polar ejecta and the tidal ejecta, and the opening angle of the shocked cocoon  $\theta_{cocoon}$ . Finally, the observer’s viewing angle  $\theta$  and the host hydrogen column density  $N_H$  are taken as parameters as well. The model is implemented in the Modular Open Source Fitter for Transients (MOSFiT; Guillochon et al. 2018), which can be used to generate light curves in various bands. We generate an ensemble of models, using the binary parameters  $\mathcal{M}$  and  $q$  from Abbott et al. (2020) inferred for

<sup>9</sup> <https://mfouesneau.github.io/pyphot/index.html>

two cases based on the spin of the neutron stars prior to merger: (1) low spin ( $\chi < 0.05$ , where  $\chi = cS/(Gm^2)$  is the dimensionless spin parameter, with  $c$  the speed of light,  $S$  the spin angular momentum magnitude and  $m$  the mass, for each component), and (2) allowing for high spin ( $\chi < 0.89$ ). The enhancement of blue ejecta due to magnetically driven winds is set to  $\alpha = 1.0$  (no enhancement), as the remnant mass is expected to lead to a prompt collapse (Nicholl et al. 2021). For the rest of the parameters, we sample 100 realizations of the ensemble (for each of the low and high spin cases) from the prior distributions that Nicholl et al. (2021) used for their GW170817 kilonova fit (which included three fixed parameters, as we repeat here). The full set of parameters and the values used are described in Table 5. The Ejecta parameters for all models are summarized in Table 6.

The comparison of reported non-detection limiting magnitudes to the GW170817 kilonova and the model light curves described above can be seen in Figure 7. The Smartt et al. (2024) split the Pan-STARRS pointings into 6209 “skycells” (see Chambers et al. 2016 for more details), each with a footprint of  $0.16 \text{ deg}^2$ , and calculated limiting magnitudes per skycell (except for the  $z$ -band observations, for which no limiting magnitudes were calculated). Here we plot each of the 6147  $i$ - and  $w$ -band skycell limits included in the 232 Pan-STARRS pointings.

We find that, had the GW190425 kilonova been similar to that of GW170817, it should have been easily detected if the entire localization region had been observed, even given the larger distance of GW190425 compared to that of GW170817. In fact, limits in the  $g$ - and  $r$ -bands are 3–4 magnitudes deeper than what would have been required to observe a GW170817-like kilonova at peak. However, given the different merger parameters, it is not clear whether the GW190425 kilonova would have been as luminous as that of GW170817. Indeed, the high lanthanide fraction Kasen et al. (2017) model predicts much fainter optical emission. According to that model, the kilonova would just have barely been detected in a few of the bands used in the search. However, the low lanthanide scenario predicts a kilonova similar to (and in the  $r$ ,  $i$  and  $z$  bands even brighter than) GW170817, which could have been detected with the observations obtained. The GW170817 kilonova could only be explained with multiple ejecta components of different opacities. If the same is true for GW190425, then the emission from its kilonova might even be as luminous as the sum of these two Kasen et al. (2017) models.

The Nicholl et al. (2021) models, which already take into account multiple ejecta components, predict a kilonova that would have been detected easily in the optical bands. This is true for both the high-spin and low-spin assumptions.

In Appendix 2, we explore an additional scenario with a “worst-case” mass ratio and cocoon geometry for the Nicholl et al. (2021) model with no blue component at all, leading to an overall redder and fainter transient compared to those in Figure 7, which would have just barely been detectable by the search.

#### 4. SUMMARY AND CONCLUSIONS

We analyzed all reported ultraviolet, optical and infrared followup observations of GW190425, the only robust BNS merger detected since GW170817, and showed that:

1. Roughly 75% of the localization region of GW190425 was accessible at the time of the trigger due to sun and moon constraints.
2. Enough observational resources were invested in the followup of GW190425 to allow the accessible part of the 90% probability region to have been covered potentially in a few hours. Instead, several regions were observed over 100 times, while others were never observed, and more than 5 days after the merger, only 50% of the probability was covered.
3. Even if the GW190425 kilonova were 3–4 magnitudes fainter than the GW170817 kilonova in its optical peak, it could still have been detected. According to more conservative models without a blue emission component, the kilonova might have been only marginally detected around peak.

Our results only take into account observations undertaken by facilities which decided to followup GW190425. We do not have information on which additional facilities preferred not to trigger given the large localization region, but which might have participated in the search, had they known that roughly half of the probability was already being covered by others.

We conclude that even for relatively distant BNS mergers with large localizations, coordinated followup can significantly increase the chances of discovering an EM counterpart. Furthermore, when no counterparts are detected, a lack of coordination weakens our ability to constrain models of kilonova emission, given the amount of localization probability that was not covered, and for which no non-detection limits are available. For smaller localizations, coordination can still help find the

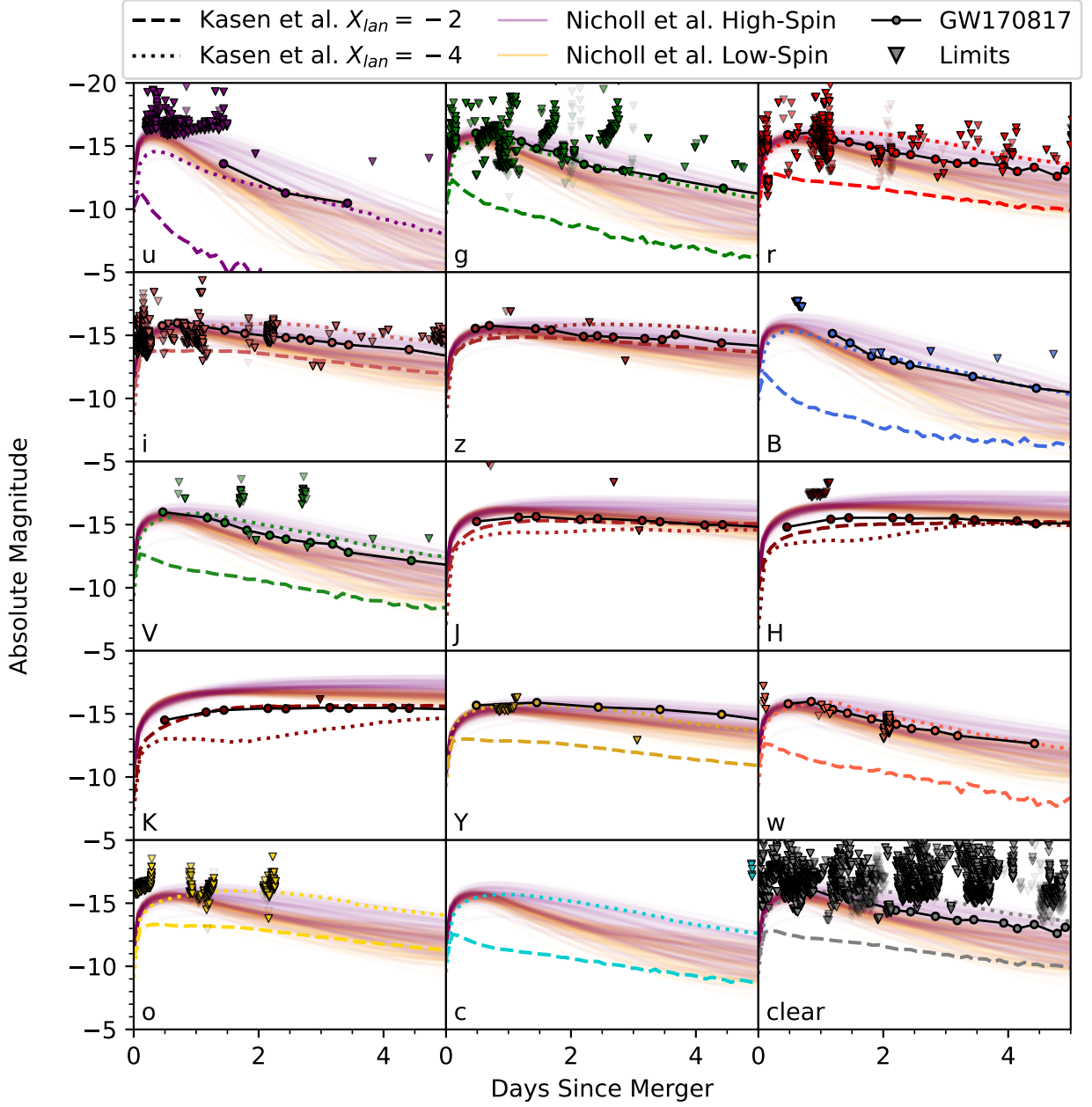


**Figure 7.**  $5\sigma$  non-detection limits of the GW190425 kilonova (triangles) compared to two kilonova models from Kasen et al. (2017) with dashed and dotted lines for  $X_{lan} = -2$  and  $X_{lan} = -4$ , respectively, two ensembles of models from Nicholl et al. (2021) with semi-transparent solid purple and orange lines for high and low spin cases, respectively, and the GW170817 kilonova (circles; see text for data sources). The upper limit triangles are displayed fully opaque for observations within the 50% GWTC-2 localization region, partially opaque for observations outside the 50% GWTC-2 localization region but within the 90% GWTC-2 localization region, and almost transparent for observations outside the 90% GWTC-2 localization region. The limits are converted to absolute magnitude after Milky Way extinction correction and using the distance estimate at the HEALPix closest to the center of the pointing for each limit. Data in the ‘clear’ band is unfiltered and is compared to models in the  $r$ -band. Limits with magnitudes brighter than -20 are not shown.

kilonova sooner. Observations on few-hour time scales are critical for constraining emission models (e.g. [Arcavi 2018](#)).

[Ackley et al. \(2020\)](#) list some of the candidate counterparts to the neutron-star - black-hole merger GW190814 and find little overlap in candidates between the different surveys, although they did overlap in the search area. This demonstrates that some overlap in observations is necessary (given different observing bands, depths and candidate search algorithms). However, such overlap should still be made as efficient as possible through co-ordination.

Real-time coordination in such a competitive field, requiring rapid response, is challenging. Tools like the **Treasure Map** have been built exactly to overcome this challenge. We encourage the community to report their pointings to the **Treasure Map**, and to use the information there to guide their search, even if it means searching lower probability areas (instead of contributing the 100th observation to a higher probability region).

With the lack of additional significant BNS merger discoveries since GW190425, it is possible that the BNS merger rate is on the lower end of its large uncertainty range, and events as nearby and well localized as GW170817 are likely very rare. If we wish to unleash the potential of GW-EM multi-messenger astronomy for nuclear physics, astrophysics, and cosmology, we must better coordinate our GW followup searches.

We thank A. Tohuvavohu, M. Nicholl, J. Gillanders, A. Levan and M. Fraser for helpful comments. We further thank A. Tohuvavohu for assisting with querying **Treasure Map** and M. Nicholl for help using the kilonova model implemented in **MOSFiT**. I.A. acknowledges support from the European Research Council (ERC) under the European Union’s Horizon 2020 research and innovation program (grant agreement number 852097), and from the Pazy foundation (grant number 216312). I.K. and I.A. acknowledge support from the Israel Science Foundation (grant number 2752/19), from the United States - Israel Binational Science Foundation (BSF; grant number 2018166). This paper has made use of version 2.3 of the **GLADE** galaxy catalog ([Dálya et al. 2018](#)), the NASA/IPAC Infrared Science Archive, which is funded by the National Aeronautics and Space Administration and operated by the California Institute of Technology ([Schlafly & Finkbeiner 2011](#)) and the **SIMBAD** database, operated at CDS, Strasbourg, France.

*Software:* `astropy` ([Astropy Collaboration et al. 2022](#)), `healpy` ([Górski et al. 2005](#)), `matplotlib` ([Hunter 2007](#)), `MOSFiT`, `numpy` ([van der Walt et al. 2011](#)), `pandas`, `pyphot`.

## REFERENCES

- Abbott, B. P., Abbott, R., Abbott, T. D., et al. 2017a, *PhRvL*, 119, 161101, doi: [10.1103/PhysRevLett.119.161101](#)
- . 2017b, *ApJL*, 848, L13, doi: [10.3847/2041-8213/aa920c](#)
- Abbott, B. P., Abbott, R., Abbott, T. D., et al. 2017, *The Astrophysical Journal Letters*, 848, L12, doi: [10.3847/2041-8213/aa91c9](#)
- Abbott, B. P., Abbott, R., Abbott, T. D., et al. 2017, *Nature*, 551, 85, doi: [10.1038/nature24471](#)
- Abbott, B. P., Abbott, R., Abbott, T. D., et al. 2020, *The Astrophysical Journal Letters*, 892, L3, doi: [10.3847/2041-8213/ab75f5](#)
- Abbott, R., Abbott, T. D., Abraham, S., & et al. 2021, *Physical Review X*, 11, 021053, doi: [10.1103/PhysRevX.11.021053](#)
- Acernese, F., Agathos, M., Agatsuma, K., et al. 2014, *Classical and Quantum Gravity*, 32, 024001, doi: [10.1088/0264-9381/32/2/024001](#)
- Ackley, K., Amati, L., Barbieri, C., et al. 2020, *A&A*, 643, A113, doi: [10.1051/0004-6361/202037669](#)
- Ahumada, T., Coughlin, M. W., Staats, K., Burdge, K., & Dekany, R. G. 2019a, *GRB Coordinates Network*, 24320, 1
- Ahumada, T., Coughlin, M. W., Staats, K., & Dekany, R. G. 2019b, *GRB Coordinates Network*, 24198, 1
- Ahumada, T., Coughlin, M. W., Staats, K., et al. 2019c, *GRB Coordinates Network*, 24343, 1
- Andreoni, I., Ackley, K., Cooke, J., et al. 2017, *PASA*, 34, e069, doi: [10.1017/pasa.2017.65](#)
- Antier, S., Agayeva, S., Aivazyan, V., et al. 2020, *MNRAS*, 492, 3904, doi: [10.1093/mnras/stz3142](#)
- Arcavi, I. 2018, *The Astrophysical Journal Letters*, 855, L23, doi: [10.3847/2041-8213/aab267](#)
- Arcavi, I., Howell, D. A., McCully, C., et al. 2019, *GRB Coordinates Network*, 24307, 1
- Arcavi, I., McCully, C., Hosseinzadeh, G., et al. 2017a, *ApJL*, 848, L33, doi: [10.3847/2041-8213/aa910f](#)
- Arcavi, I., Hosseinzadeh, G., Howell, D. A., et al. 2017b, *Nature*, 551, 64, doi: [10.1038/nature24291](#)

- Astropy Collaboration, Price-Whelan, A. M., Lim, P. L., et al. 2022, *ApJ*, 935, 167, doi: [10.3847/1538-4357/ac7c74](https://doi.org/10.3847/1538-4357/ac7c74)
- Atwood, W. B., Abdo, A. A., Ackermann, M., et al. 2009, *ApJ*, 697, 1071, doi: [10.1088/0004-637X/697/2/1071](https://doi.org/10.1088/0004-637X/697/2/1071)
- Axelsson, M., Omodei, N., Kocevski, D., & Longo, F. 2019, *GRB Coordinates Network*, 24174, 1
- Barnes, J., & Kasen, D. 2013, *The Astrophysical Journal*, 775, 18, doi: [10.1088/0004-637X/775/1/18](https://doi.org/10.1088/0004-637X/775/1/18)
- Bauswein, A., Goriely, S., & Janka, H. T. 2013, *ApJ*, 773, 78, doi: [10.1088/0004-637X/773/1/78](https://doi.org/10.1088/0004-637X/773/1/78)
- Becerra, R. L., Dichiara, S., Watson, A. M., et al. 2021, *MNRAS*, 507, 1401, doi: [10.1093/mnras/stab2086](https://doi.org/10.1093/mnras/stab2086)
- Bhalerao, V., Kumar, H., Karambelkar, V., et al. 2019, *GRB Coordinates Network*, 24201, 1
- Blazek, M., Christensen, N., Howell, E., et al. 2019, *GRB Coordinates Network*, 24227, 1
- Bloom, J. S., Zucker, C., Schlafly, E., et al. 2019, *GRB Coordinates Network*, 24337, 1
- Boër, M., Bringer, M., Klotz, A., et al. 1999, *A&AS*, 138, 579, doi: [10.1051/aas:1999356](https://doi.org/10.1051/aas:1999356)
- Bowen, I. S., & Vaughan, A. H., J. 1973, *ApOpt*, 12, 1430, doi: [10.1364/AO.12.001430](https://doi.org/10.1364/AO.12.001430)
- Brown, T. M., Baliber, N., Bianco, F. B., et al. 2013, *PASP*, 125, 1031, doi: [10.1086/673168](https://doi.org/10.1086/673168)
- Burke, J., Hiramatsu, D., Arcavi, I., et al. 2019, *GRB Coordinates Network*, 24206, 1
- Butler, N., Watson, A. M., Troja, E., et al. 2019, *GRB Coordinates Network*, 24238, 1
- Camilletti, A., Chiesa, L., Ricigliano, G., et al. 2022, *Monthly Notices of the Royal Astronomical Society*, 516, 4760, doi: [10.1093/mnras/stac2333](https://doi.org/10.1093/mnras/stac2333)
- Castro-Tirado, A. J., Hu, Y. D., Li, X. Y., et al. 2019, *GRB Coordinates Network*, 24214, 1
- Chambers, K. C., Magnier, E. A., Metcalfe, N., et al. 2016, *arXiv e-prints*, arXiv:1612.05560, doi: [10.48550/arXiv.1612.05560](https://doi.org/10.48550/arXiv.1612.05560)
- Chang, S. W., Wolf, C., Onken, C. A., Luvaul, L., & Scott, S. 2019, *GRB Coordinates Network*, 24325, 1
- Clark, J. P. A., & Eardley, D. M. 1977, *ApJ*, 215, 311, doi: [10.1086/155360](https://doi.org/10.1086/155360)
- Cobos, F. J., Gonzalez, J. J., Tejada, C., Cepa, J., & Rasilla, J. L. 2002, in *Society of Photo-Optical Instrumentation Engineers (SPIE) Conference Series*, Vol. 4832, *Society of Photo-Optical Instrumentation Engineers (SPIE) Conference Series*, 249–257, doi: [10.1117/12.486467](https://doi.org/10.1117/12.486467)
- Coulter, D. A., Kilpatrick, C. D., Siebert, M. R., et al. 2017a, *GRB Coordinates Network*, 21529, 1
- Coulter, D. A., Foley, R. J., Kilpatrick, C. D., et al. 2017b, *Science*, 358, 1556, doi: [10.1126/science.aap9811](https://doi.org/10.1126/science.aap9811)
- Coulter, D. A., Kilpatrick, C. D., Jones, D. O., et al. 2024, *arXiv e-prints*, arXiv:2404.15441, doi: [10.48550/arXiv.2404.15441](https://doi.org/10.48550/arXiv.2404.15441)
- Cowperthwaite, P. S., Berger, E., Villar, V. A., et al. 2017, *ApJL*, 848, L17, doi: [10.3847/2041-8213/aa8fc7](https://doi.org/10.3847/2041-8213/aa8fc7)
- Dalton, G. B., Caldwell, M., Ward, A. K., et al. 2006, in *Society of Photo-Optical Instrumentation Engineers (SPIE) Conference Series*, Vol. 6269, *Society of Photo-Optical Instrumentation Engineers (SPIE) Conference Series*, ed. I. S. McLean & M. Iye, 62690X, doi: [10.1117/12.670018](https://doi.org/10.1117/12.670018)
- Dálya, G., Galgóczi, G., Dobos, L., et al. 2018, *MNRAS*, 479, 2374, doi: [10.1093/mnras/sty1703](https://doi.org/10.1093/mnras/sty1703)
- DePoy, D. L., Atwood, B., Belville, S. R., et al. 2003, in *Society of Photo-Optical Instrumentation Engineers (SPIE) Conference Series*, Vol. 4841, *Instrument Design and Performance for Optical/Infrared Ground-based Telescopes*, ed. M. Iye & A. F. M. Moorwood, 827–838, doi: [10.1117/12.459907](https://doi.org/10.1117/12.459907)
- Díaz, M. C., Macri, L. M., Garcia Lambas, D., et al. 2017, *ApJL*, 848, L29, doi: [10.3847/2041-8213/aa9060](https://doi.org/10.3847/2041-8213/aa9060)
- Djupvik, A. A., & Andersen, J. 2010, in *Astrophysics and Space Science Proceedings*, Vol. 14, *Highlights of Spanish Astrophysics V*, 211, doi: [10.1007/978-3-642-11250-8\\_21](https://doi.org/10.1007/978-3-642-11250-8_21)
- Drake, A. J., Djorgovski, S. G., Mahabal, A., et al. 2009, *ApJ*, 696, 870, doi: [10.1088/0004-637X/696/1/870](https://doi.org/10.1088/0004-637X/696/1/870)
- Drout, M. R., Piro, A. L., Shappee, B. J., et al. 2017, *Science*, 358, 1570, doi: [10.1126/science.aaq0049](https://doi.org/10.1126/science.aaq0049)
- Dudi, R., Adhikari, A., Brüggemann, B., et al. 2022, *Phys. Rev. D*, 106, 084039, doi: [10.1103/PhysRevD.106.084039](https://doi.org/10.1103/PhysRevD.106.084039)
- Dyer, M. J., Ackley, K., Lyman, J., et al. 2022, in *Society of Photo-Optical Instrumentation Engineers (SPIE) Conference Series*, Vol. 12182, *Ground-based and Airborne Telescopes IX*, ed. H. K. Marshall, J. Spyromilio, & T. Usuda, 121821Y, doi: [10.1117/12.2629369](https://doi.org/10.1117/12.2629369)
- Eichler, D., Livio, M., Piran, T., & Schramm, D. N. 1989, *Nature*, 340, 126, doi: [10.1038/340126a0](https://doi.org/10.1038/340126a0)
- Emerson, J., McPherson, A., & Sutherland, W. 2006, *The Messenger*, 126, 41
- Evans, P. A., Cenko, S. B., Kennea, J. A., et al. 2017, *Science*, 358, 1565, doi: [10.1126/science.aap9580](https://doi.org/10.1126/science.aap9580)
- Fabricant, D., Fata, R., Epps, H., et al. 2019, *PASP*, 131, 075004, doi: [10.1088/1538-3873/ab1d78](https://doi.org/10.1088/1538-3873/ab1d78)
- Farah, A., Barojas, E., Butler, N. R., et al. 2010, in *Society of Photo-Optical Instrumentation Engineers (SPIE) Conference Series*, Vol. 7735, *Ground-based and Airborne Instrumentation for Astronomy III*, ed. I. S. McLean, S. K. Ramsay, & H. Takami, 77357Z, doi: [10.1117/12.857828](https://doi.org/10.1117/12.857828)

- Filippenko, A. V., Li, W. D., Treffers, R. R., & Modjaz, M. 2001, in *Astronomical Society of the Pacific Conference Series*, Vol. 246, IAU Colloq. 183: Small Telescope Astronomy on Global Scales, ed. B. Paczynski, W.-P. Chen, & C. Lemme, 121
- Flaugher, B., Diehl, H. T., Honscheid, K., et al. 2015, *AJ*, 150, 150, doi: [10.1088/0004-6256/150/5/150](https://doi.org/10.1088/0004-6256/150/5/150)
- Fletcher, C., Fermi-GBM Team, & GBM-LIGO/Virgo Group. 2019, *GRB Coordinates Network*, 24185, 1
- Foley, R. J., Coulter, D. A., Kilpatrick, C. D., et al. 2020, *Monthly Notices of the Royal Astronomical Society*, 494, 190, doi: [10.1093/mnras/staa725](https://doi.org/10.1093/mnras/staa725)
- Foley, R. J., Coulter, D. A., Kilpatrick, C. D., et al. 2020, *MNRAS*, 494, 190, doi: [10.1093/mnras/staa725](https://doi.org/10.1093/mnras/staa725)
- Gehrels, N., Chincarini, G., Giommi, P., et al. 2004, *ApJ*, 611, 1005, doi: [10.1086/422091](https://doi.org/10.1086/422091)
- Gompertz, B. P., Cutter, R., Steeghs, D., et al. 2020, *MNRAS*, 497, 726, doi: [10.1093/mnras/staa1845](https://doi.org/10.1093/mnras/staa1845)
- Górski, K. M., Hivon, E., Banday, A. J., et al. 2005, *ApJ*, 622, 759, doi: [10.1086/427976](https://doi.org/10.1086/427976)
- Greiner, J., Bornemann, W., Clemens, C., et al. 2008, *PASP*, 120, 405, doi: [10.1086/587032](https://doi.org/10.1086/587032)
- Grossman, D., Korobkin, O., Rosswog, S., & Piran, T. 2014, *Monthly Notices of the Royal Astronomical Society*, 439, 757, doi: [10.1093/mnras/stt2503](https://doi.org/10.1093/mnras/stt2503)
- Guillochon, J., Nicholl, M., Villar, V. A., et al. 2018, *ApJS*, 236, 6, doi: [10.3847/1538-4365/aab761](https://doi.org/10.3847/1538-4365/aab761)
- Guo, B., Peng, Q., Chen, Y., et al. 2022, *Research in Astronomy and Astrophysics*, 22, 055007, doi: [10.1088/1674-4527/ac5959](https://doi.org/10.1088/1674-4527/ac5959)
- Han, W., Mack, P., Lee, C.-U., et al. 2005, *PASJ*, 57, 821, doi: [10.1093/pasj/57.5.821](https://doi.org/10.1093/pasj/57.5.821)
- Han, X., Xiao, Y., Zhang, P., et al. 2021, *Publications of the Astronomical Society of the Pacific*, 133, 065001, doi: [10.1088/1538-3873/abfb4e](https://doi.org/10.1088/1538-3873/abfb4e)
- Hiramatsu, D., Arcavi, I., Burke, J., et al. 2019a, *GRB Coordinates Network*, 24194, 1
- Hiramatsu, D., Pellegrino, C., Burke, J., et al. 2019b, *GRB Coordinates Network*, 24225, 1
- Hosseinzadeh, G., Cowperthwaite, P. S., Gomez, S., et al. 2019a, *ApJL*, 880, L4, doi: [10.3847/2041-8213/ab271c](https://doi.org/10.3847/2041-8213/ab271c)
- Hosseinzadeh, G., Berger, E., Blanchard, P. K., et al. 2019b, *GRB Coordinates Network*, 24182, 1
- Hotokezaka, K., Kiuchi, K., Kyutoku, K., et al. 2013, *Phys. Rev. D*, 87, 024001, doi: [10.1103/PhysRevD.87.024001](https://doi.org/10.1103/PhysRevD.87.024001)
- Howell, E., Christensen, N., Blazek, M., et al. 2019, *GRB Coordinates Network*, 24256, 1
- Hu, L., Wu, X., Andreoni, I., et al. 2017, *Science Bulletin*, 62, 1433, doi: [10.1016/j.scib.2017.10.006](https://doi.org/10.1016/j.scib.2017.10.006)
- Hu, Y. D., Li, X. Y., Carrasco, I., et al. 2019a, *GRB Coordinates Network*, 24270, 1
- Hu, Y. D., Castro-Tirado, A. J., Li, X. Y., et al. 2019b, *GRB Coordinates Network*, 24324, 1
- Hunter, J. D. 2007, *Computing in Science and Engineering*, 9, 90, doi: [10.1109/MCSE.2007.55](https://doi.org/10.1109/MCSE.2007.55)
- Im, M., Paek, G. S. H., Lim, G., et al. 2019, *GRB Coordinates Network*, 24183, 1
- Izzo, L., Malesani, D. B., & Carini, R. 2019, *GRB Coordinates Network*, 24319, 1
- Kann, D. A., Thoene, C., Stachie, C., et al. 2019, *GRB Coordinates Network*, 24459, 1
- Kasen, D., Badnell, N. R., & Barnes, J. 2013, *The Astrophysical Journal*, 774, 25, doi: [10.1088/0004-637X/774/1/25](https://doi.org/10.1088/0004-637X/774/1/25)
- Kasen, D., Metzger, B., Barnes, J., Quataert, E., & Ramirez-Ruiz, E. 2017, *Nature*, 551, 80, doi: [10.1038/nature24453](https://doi.org/10.1038/nature24453)
- Kashikawa, N., Aoki, K., Asai, R., et al. 2002, *PASJ*, 54, 819, doi: [10.1093/pasj/54.6.819](https://doi.org/10.1093/pasj/54.6.819)
- Kasliwal, M. M., Nakar, E., Singer, L. P., et al. 2017, *Science*, 358, 1559, doi: [10.1126/science.aap9455](https://doi.org/10.1126/science.aap9455)
- Kasliwal, M. M., Cannella, C., Bagdasaryan, A., et al. 2019, *PASP*, 131, 038003, doi: [10.1088/1538-3873/aafbc2](https://doi.org/10.1088/1538-3873/aafbc2)
- Keller, S. C., Schmidt, B. P., Bessell, M. S., et al. 2007, *PASA*, 24, 1, doi: [10.1071/AS07001](https://doi.org/10.1071/AS07001)
- Kim, J., Im, M., Lee, C. U., et al. 2019, *GRB Coordinates Network*, 24216, 1
- Kim, S.-L., Lee, C.-U., Park, B.-G., et al. 2016, *Journal of Korean Astronomical Society*, 49, 37, doi: [10.5303/JKAS.2016.49.1.37](https://doi.org/10.5303/JKAS.2016.49.1.37)
- Kong, A. 2019, *GRB Coordinates Network*, 24303, 1
- Kulkarni, S. R. 2005, *arXiv e-prints*, astro, doi: [10.48550/arXiv.astro-ph/0510256](https://doi.org/10.48550/arXiv.astro-ph/0510256)
- Kyutoku, K., Fujibayashi, S., Hayashi, K., et al. 2020, *ApJL*, 890, L4, doi: [10.3847/2041-8213/ab6e70](https://doi.org/10.3847/2041-8213/ab6e70)
- Li, B., Xu, D., Zhou, X., & Lu, H. 2019a, *GRB Coordinates Network*, 24285, 1
- Li, L.-X., & Paczyński, B. 1998, *The Astrophysical Journal*, 507, L59, doi: [10.1086/311680](https://doi.org/10.1086/311680)
- Li, W. X., Chen, J. C., Xiaofeng, W. X., et al. 2019b, *GRB Coordinates Network*, 24267, 1
- Ligo Scientific Collaboration, & VIRGO Collaboration. 2019a, *GRB Coordinates Network*, 24168, 1
- . 2019b, *GRB Coordinates Network*, 24228, 1
- LIGO Scientific Collaboration, T., Aasi, J., Abbott, B. P., et al. 2015, *Classical and Quantum Gravity*, 32, 074001, doi: [10.1088/0264-9381/32/7/074001](https://doi.org/10.1088/0264-9381/32/7/074001)



- Lipunov, V., Kornilov, V., Gorbovskoy, E., et al. 2010, *Advances in Astronomy*, 2010, 349171, doi: [10.1155/2010/349171](https://doi.org/10.1155/2010/349171)
- Lipunov, V. M., Gorbovskoy, E., Kornilov, V. G., et al. 2017, *ApJL*, 850, L1, doi: [10.3847/2041-8213/aa92c0](https://doi.org/10.3847/2041-8213/aa92c0)
- Lundquist, M. J., Paterson, K., Fong, W., et al. 2019, *ApJL*, 881, L26, doi: [10.3847/2041-8213/ab32f2](https://doi.org/10.3847/2041-8213/ab32f2)
- Margutti, R., & Chornock, R. 2021, *ARA&A*, 59, 155, doi: [10.1146/annurev-astro-112420-030742](https://doi.org/10.1146/annurev-astro-112420-030742)
- Masci, F. J., Laher, R. R., Rusholme, B., et al. 2018, *Publications of the Astronomical Society of the Pacific*, 131, 018003, doi: [10.1088/1538-3873/aae8ac](https://doi.org/10.1088/1538-3873/aae8ac)
- Meegan, C., Lichti, G., Bhat, P. N., et al. 2009, *The Astrophysical Journal*, 702, 791, doi: [10.1088/0004-637X/702/1/791](https://doi.org/10.1088/0004-637X/702/1/791)
- Metzger, B. D., Martínez-Pinedo, G., Darbha, S., et al. 2010, *Monthly Notices of the Royal Astronomical Society*, 406, 2650, doi: [10.1111/j.1365-2966.2010.16864.x](https://doi.org/10.1111/j.1365-2966.2010.16864.x)
- Morihana, K., Jian, M., & Nagayama, T. 2019a, *GRB Coordinates Network*, 24219, 1
- . 2019b, *GRB Coordinates Network*, 24328, 1
- Nagayama, T., Nagashima, C., Nakajima, Y., et al. 2003, in *Society of Photo-Optical Instrumentation Engineers (SPIE) Conference Series*, Vol. 4841, *Instrument Design and Performance for Optical/Infrared Ground-based Telescopes*, ed. M. Iye & A. F. M. Moorwood, 459–464, doi: [10.1117/12.460770](https://doi.org/10.1117/12.460770)
- Nakar, E. 2020, *PhR*, 886, 1, doi: [10.1016/j.physrep.2020.08.008](https://doi.org/10.1016/j.physrep.2020.08.008)
- Nakar, E., & Piran, T. 2016, *The Astrophysical Journal*, 834, 28, doi: [10.3847/1538-4357/834/1/28](https://doi.org/10.3847/1538-4357/834/1/28)
- Nicholl, M., Margalit, B., Schmidt, P., et al. 2021, *MNRAS*, 505, 3016, doi: [10.1093/mnras/stab1523](https://doi.org/10.1093/mnras/stab1523)
- Nicholl, M., Margalit, B., Schmidt, P., et al. 2021, *Monthly Notices of the Royal Astronomical Society*, 505, 3016, doi: [10.1093/mnras/stab1523](https://doi.org/10.1093/mnras/stab1523)
- Nicholl, M., Margalit, B., Schmidt, P., et al. 2021, *MNRAS*, 505, 3016, doi: [10.1093/mnras/stab1523](https://doi.org/10.1093/mnras/stab1523)
- Paek, G. S. H., Im, M., Lim, G., et al. 2019, *GRB Coordinates Network*, 24188, 1
- Park, W.-K., Pak, S., Im, M., et al. 2012, *PASP*, 124, 839, doi: [10.1086/667390](https://doi.org/10.1086/667390)
- Perley, D. A., & Copperwheat, C. M. 2019, *GRB Coordinates Network*, 24202, 1
- Perley, D. A., Copperwheat, C. M., & Taggart, K. L. 2019, *GRB Coordinates Network*, 24314, 1
- Pian, E., D’Avanzo, P., Benetti, S., et al. 2017, *Nature*, 551, 67, doi: [10.1038/nature24298](https://doi.org/10.1038/nature24298)
- Piro, A. L., & Kollmeier, J. A. 2018, *ApJ*, 855, 103, doi: [10.3847/1538-4357/aaaab3](https://doi.org/10.3847/1538-4357/aaaab3)
- Pozanenko, A. S., Minaev, P. Y., Grebenev, S. A., & Chelovekov, I. V. 2020, *Astronomy Letters*, 45, 710, doi: [10.1134/S1063773719110057](https://doi.org/10.1134/S1063773719110057)
- Pozanenko, A. S., Barkov, M. V., Minaev, P. Y., et al. 2018, *ApJL*, 852, L30, doi: [10.3847/2041-8213/aaa2f6](https://doi.org/10.3847/2041-8213/aaa2f6)
- Radice, D., Ricigliano, G., Bhattacharya, M., et al. 2024, *Monthly Notices of the Royal Astronomical Society*, 528, 5836, doi: [10.1093/mnras/stae400](https://doi.org/10.1093/mnras/stae400)
- Roming, P. W. A., Kennedy, T. E., Mason, K. O., et al. 2005, *SSRv*, 120, 95, doi: [10.1007/s11214-005-5095-4](https://doi.org/10.1007/s11214-005-5095-4)
- Rosswog, S., Liebendörfer, M., Thielemann, F. K., et al. 1999, *A&A*, 341, 499, doi: [10.48550/arXiv.astro-ph/9811367](https://doi.org/10.48550/arXiv.astro-ph/9811367)
- Sagués Carracedo, A., Bulla, M., Feindt, U., & Goobar, A. 2021, *MNRAS*, 504, 1294, doi: [10.1093/mnras/stab872](https://doi.org/10.1093/mnras/stab872)
- Sakamoto, T., Barthelmy, S. D., Lien, A. Y., et al. 2019, *GRB Coordinates Network*, 24184, 1
- Sasada, M., Akitaya, H., Nakaoka, T., et al. 2019, *GRB Coordinates Network*, 24192, 1
- Savchenko, V., Ferrigno, C., Martin-Carillo, A., et al. 2019, *GRB Coordinates Network*, 24178, 1
- Schady, P., Chen, T. W., Schweyer, T., Malesani, D. B., & Bolmer, J. 2019, *GRB Coordinates Network*, 24229, 1
- Schechter, P. 1976, *ApJ*, 203, 297, doi: [10.1086/154079](https://doi.org/10.1086/154079)
- Schlafly, E. F., & Finkbeiner, D. P. 2011, *ApJ*, 737, 103, doi: [10.1088/0004-637X/737/2/103](https://doi.org/10.1088/0004-637X/737/2/103)
- Shappee, B. J., Simon, J. D., Drout, M. R., et al. 2017, *Science*, 358, 1574, doi: [10.1126/science.aaq0186](https://doi.org/10.1126/science.aaq0186)
- Smartt, S. J., Chen, T. W., Jerkstrand, A., et al. 2017, *Nature*, 551, 75, doi: [10.1038/nature24303](https://doi.org/10.1038/nature24303)
- Smartt, S. J., Nicholl, M., Srivastav, S., et al. 2024, *MNRAS*, 528, 2299, doi: [10.1093/mnras/stae100](https://doi.org/10.1093/mnras/stae100)
- Steele, I. A., Smith, R. J., Rees, P. C., et al. 2004, in *Society of Photo-Optical Instrumentation Engineers (SPIE) Conference Series*, Vol. 5489, *Ground-based Telescopes*, ed. J. Oschmann, Jacobus M., 679–692, doi: [10.1117/12.551456](https://doi.org/10.1117/12.551456)
- Sun, T., Chen, J., Hu, L., et al. 2019, *GRB Coordinates Network*, 24234, 1
- Swift, J. J., Andersen, K., Arculli, T., et al. 2022, *Publications of the Astronomical Society of the Pacific*, 134, 035005, doi: [10.1088/1538-3873/ac5aca](https://doi.org/10.1088/1538-3873/ac5aca)
- Tan, H. J., Yu, P. C., Ngeow, C. C., & Ip, W. H. 2019a, *GRB Coordinates Network*, 24193, 1
- Tan, H. J., Yu, P. C., Patil, A. S., et al. 2019b, *GRB Coordinates Network*, 24274, 1
- Tanaka, M., & Hotokezaka, K. 2013, *The Astrophysical Journal*, 775, 113, doi: [10.1088/0004-637X/775/2/113](https://doi.org/10.1088/0004-637X/775/2/113)

- Tanvir, N. R., Gonzalez-Fernandez, C., Levan, A. J., Malesani, D. B., & Evans, P. A. 2019, GRB Coordinates Network, 24334, 1
- Tanvir, N. R., Levan, A. J., González-Fernández, C., et al. 2017, *ApJL*, 848, L27, doi: [10.3847/2041-8213/aa90b6](https://doi.org/10.3847/2041-8213/aa90b6)
- Tonry, J. L., Denneau, L., Heinze, A. N., et al. 2018, *PASP*, 130, 064505, doi: [10.1088/1538-3873/aabadf](https://doi.org/10.1088/1538-3873/aabadf)
- Troja, E., Piro, L., van Eerten, H., et al. 2017, *Nature*, 551, 71, doi: [10.1038/nature24290](https://doi.org/10.1038/nature24290)
- Troja, E., Watson, A. M., Becerra, R. L., et al. 2019, GRB Coordinates Network, 24335, 1
- Utsumi, Y., Tanaka, M., Tominaga, N., et al. 2017, *PASJ*, 69, 101, doi: [10.1093/pasj/psx118](https://doi.org/10.1093/pasj/psx118)
- Valenti, S., Sand, D. J., Yang, S., et al. 2017, *ApJL*, 848, L24, doi: [10.3847/2041-8213/aa8edf](https://doi.org/10.3847/2041-8213/aa8edf)
- van der Walt, S., Colbert, S. C., & Varoquaux, G. 2011, *Computing in Science and Engineering*, 13, 22, doi: [10.1109/MCSE.2011.37](https://doi.org/10.1109/MCSE.2011.37)
- Vinko, A., Bodi, L., Kriskovics, K., Sarneczky, K., & Pal, A. 2019, GRB Coordinates Network, 24367, 1
- Wang, C.-J., Bai, J.-M., Fan, Y.-F., et al. 2019, *Research in Astronomy and Astrophysics*, 19, 149, doi: [10.1088/1674-4527/19/10/149](https://doi.org/10.1088/1674-4527/19/10/149)
- Waratkar, G., Kumar, H., Bhalerao, V., Stanzin, J., & Anupama, G. C. 2019, GRB Coordinates Network, 24304, 1
- Watson, A. M., Cuevas Cardona, S., Alvarez Nuñez, L. C., et al. 2016a, in *Society of Photo-Optical Instrumentation Engineers (SPIE) Conference Series*, Vol. 9908, *Ground-based and Airborne Instrumentation for Astronomy VI*, ed. C. J. Evans, L. Simard, & H. Takami, 99085O, doi: [10.1117/12.2233000](https://doi.org/10.1117/12.2233000)
- Watson, A. M., Lee, W. H., Troja, E., et al. 2016b, in *Society of Photo-Optical Instrumentation Engineers (SPIE) Conference Series*, Vol. 9910, *Observatory Operations: Strategies, Processes, and Systems VI*, ed. A. B. Peck, R. L. Seaman, & C. R. Benn, 99100G, doi: [10.1117/12.2232898](https://doi.org/10.1117/12.2232898)
- Watson, A. M., Butler, N., Troja, E., et al. 2019, GRB Coordinates Network, 24239, 1
- Waxman, E., Ofek, E. O., Kushnir, D., & Gal-Yam, A. 2018, *MNRAS*, 481, 3423, doi: [10.1093/mnras/sty2441](https://doi.org/10.1093/mnras/sty2441)
- Wenger, M., Ochsenbein, F., Egret, D., et al. 2000, *A&AS*, 143, 9, doi: [10.1051/aas:2000332](https://doi.org/10.1051/aas:2000332)
- Winkler, C., Courvoisier, T. J. L., Di Cocco, G., et al. 2003, *A&A*, 411, L1, doi: [10.1051/0004-6361:20031288](https://doi.org/10.1051/0004-6361:20031288)
- Wyatt, S. D., Tohuvavohu, A., Arcavi, I., et al. 2020, *ApJ*, 894, 127, doi: [10.3847/1538-4357/ab855e](https://doi.org/10.3847/1538-4357/ab855e)
- Xin, L. P., Han, X. H., Wei, J. Y., et al. 2019, GRB Coordinates Network, 24315, 1
- Xu, D., Zhu, Z. P., Yu, B. Y., et al. 2019, GRB Coordinates Network, 24190, 1
- Yoshida, M., Shimizu, Y., Sasaki, T., et al. 2000, in *Society of Photo-Optical Instrumentation Engineers (SPIE) Conference Series*, Vol. 4009, *Advanced Telescope and Instrumentation Control Software*, ed. H. Lewis, 240–249, doi: [10.1117/12.388394](https://doi.org/10.1117/12.388394)
- Zheng, W., Zhang, K., Vasylyev, S., & Filippenko, A. V. 2019, GRB Coordinates Network, 24179, 1

## APPENDIX

## A. HEALPY EXCLUSIVE VS. INCLUSIVE METHODS

We present an illustration of the inclusive vs. the exclusive methods of `healpy` pixel queries in Figure 8. The inclusive method can significantly overestimate the area covered by a footprint with a field of view smaller than the pixel size. The exclusive method is much more conservative, and hence we chose it for our analysis.

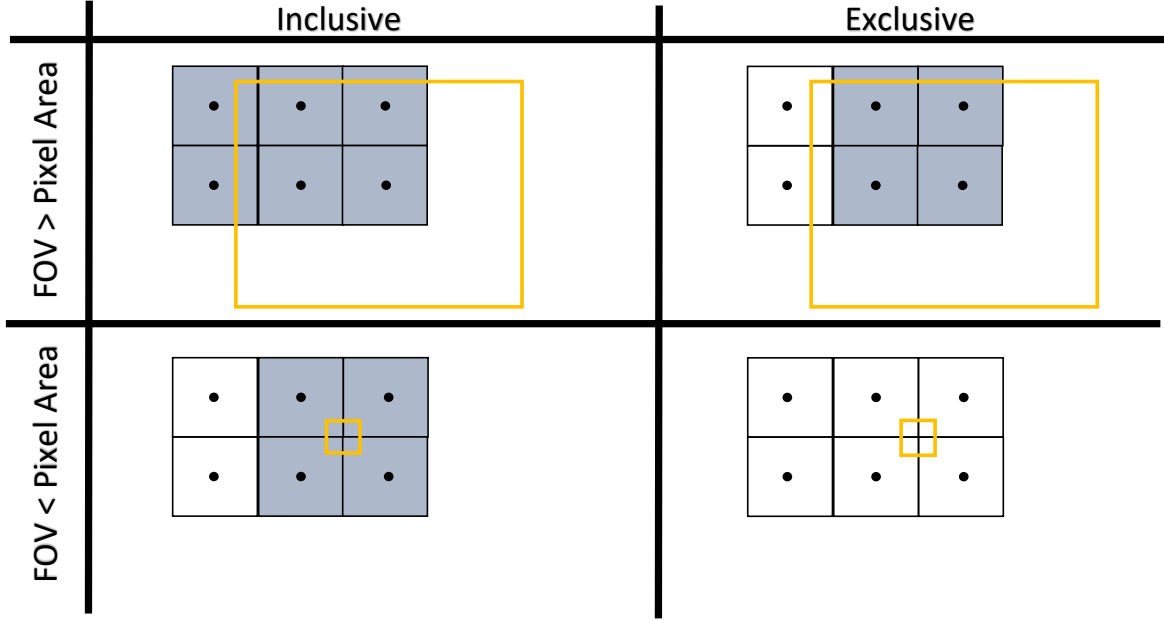


**Figure 8.** An illustration of the exclusive and inclusive `healpy` pixel query methods. Each black square represents a pixel centered around a black dot and the yellow rectangles are hypothetical observational footprints. Grey pixels are the ones returned according to each method and white pixels are ignored. The inclusive method (left) returns every pixel that intersects with the observed footprint, while the exclusive method (right) returns only pixels with centers included in the observed footprint. For footprints with a field of view (FOV) much smaller than the pixel area (bottom), the inclusive method can significantly overestimate the area covered.

## 2. ADDITIONAL KILONOVA MODELS WITH DIFFERENT PARAMETERS

We present an additional “worse case scenario” for the [Nicholl et al. \(2021\)](#) kilonova models (Figure 9). We use a mass ratio of  $0.4 < q < 0.8$  and a cocoon opening angle of  $\cos\theta_{\text{cocoon}} = 1.0$ . The rest of the parameters are the same as those in Table 5. This results in a redder and dimmer kilonova prediction with the following ejecta parameters for the red ejecta:  $M_{ej,red} = 0.0543 \pm 0.0043 M_{\odot}$  and  $v_{k,red} = 0.2628 \pm 0.0020c$ , and for the purple ejecta:  $M_{ej,purple} = 0.00275 \pm 0.00041 M_{\odot}$ ,  $v_{k,purple} = 0.0453 \pm 0.0010c$  and  $\kappa_{ej,purple} \simeq 5.6 \text{ cm}^2/g$ , with no blue component.

The total ejecta mass of  $M_{ej} = 0.0570 \pm 0.0041 M_{\odot}$  has an opacity of  $\kappa_{ej} \simeq 9.5 \text{ cm}^2/g$ . Such a kilonova would have been marginally detectable with some of the observations obtained.

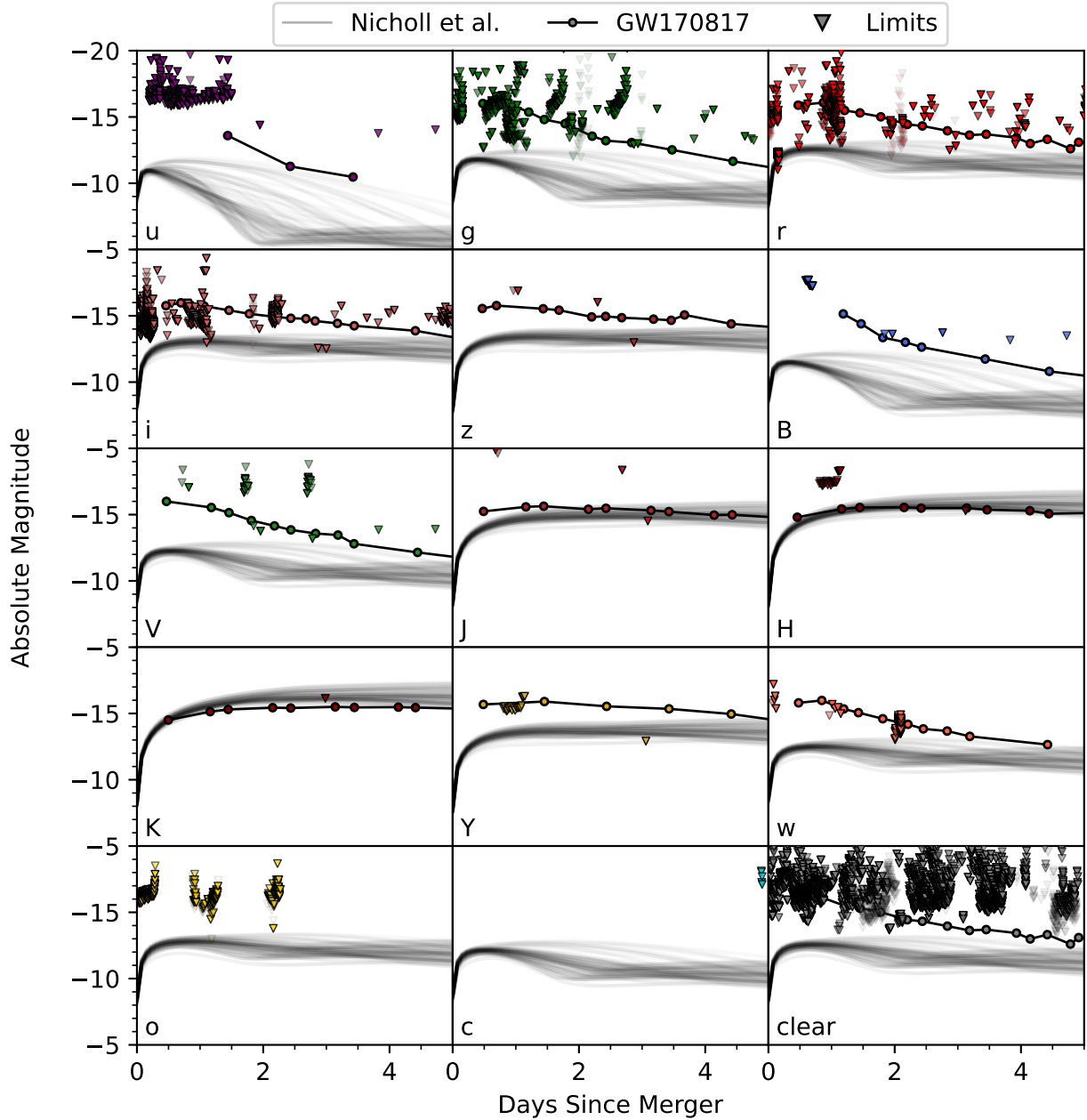


**Figure 9.** Same as Figure 7, but with a “worst-case” Nicholl et al. (2021) model ensemble.